Redox-Active Mesomorphic Complexes from the Ionic Self-Assembly of Cationic Polyferrocenylsilane Polyelectrolytes and Anionic Surfactants

ARTICLE *in* SOFT MATTER · NOVEMBER 2011

Impact Factor: 4.03 · DOI: 10.1039/C1SM06374J

6 AUTHORS, INCLUDING:

Ming-Siao Hsiao
Air Force Research Laboratory, WPAFB
22 PUBLICATIONS **307** CITATIONS
SEE PROFILE

Nikolay Houbenov
Aalto University
33 PUBLICATIONS **1,080** CITATIONS
SEE PROFILE

Charl FJ Faul
University of Bristol
87 PUBLICATIONS **2,112** CITATIONS
SEE PROFILE

Soft Matter

View Online
Dynamic Article Links

Cite this: *Soft Matter*, 2011, **7**, 10462

www.rsc.org/softmatter

PAPER

Redox-active mesomorphic complexes from the ionic self-assembly of cationic polyferrocenylsilane polyelectrolytes and anionic surfactants

Rumman Ahmed,[a] Ming-Siao Hsiao,[a] Yukihito Matsuura,[b] Nikolay Houbenov,[c] Charl F. J. Faul*[a] and Ian Manners*[a]

Received 20th July 2011, Accepted 1st September 2011
DOI: 10.1039/c1sm06374j

The concept of ionic self-assembly (ISA) has been employed to design and prepare new redox-active thermotropic liquid-crystalline materials. These ordered anisotropic materials in the bulk state were constructed from the complexation of a series of polyferrocenylsilane (PFS) polyelectrolytes with several oppositely charged surfactants. The structural characterization of the self-assembled materials was performed using a variety of techniques including FTIR, thermogravimetric analysis (TGA), differential scanning calorimetry (DSC), polarized optical microscopy (POM), small- and wide-angle X-ray scattering (SAXS and WAXS), transmission electron microscopy (TEM) and UV-vis spectroscopy. Results showed that strong coulombic attractions between the starting building blocks resulted in the formation of ordered mesostructures with average periodicities of 2–3 nm. The precise phase thickness of both the PFS and surfactant layers was quantitatively determined using a one-dimensional correlation function. Moreover, the redox properties of the mesomorphic organometallic PFS polyelectrolyte–surfactant complexes were systematically investigated using cyclic voltammetry (CV) and chemical redox methods. The versatility of this ISA technique also allowed the incorporation of a photoactive azobenzene-containing surfactant, resulting in ordered mesostructures with potential optoelectronic applications.

1. Introduction

As a result of their facile synthesis, structural versatility, and potential applications, polyelectrolyte–surfactant complexes have been of intense interest over the last decade.[1–8] Central to this theme is the technique of Ionic Self-Assembly (ISA), a powerful tool that utilizes molecular building blocks (or tectons), such as ionic surfactants and oppositely charged polyelectrolytes, to form new nanostructures and functional materials.[9] Usually, ionic binding of the surfactant molecules to the oppositely charged polyelectrolyte is characterized by cooperativity and is initiated at the critical aggregation concentration (CAC), a few orders of magnitude below the critical micelle concentration (CMC) of the surfactant itself.[10] As soon as the first electrostatic binding occurs, a highly cooperative 'zipper mechanism' takes place as a result of favourable secondary interactions amongst the hydrophobictails. The interactions observed for solid-state polyelectrolyte–surfactant complexes resemble those present in comb-like polymers,[11] and usually result in the formation of organized mesomorphic phases. This facile route allows the preparation of a wide range of organized functional materials at the nanoscale as it combines the excellent self-assembly properties of the surfactants along with the mechanical properties of the polyelectrolyte. The stoichiometry of the complexes (with respect to charge) can be tailored by changing the ratio of the polyelectrolyte to the surfactant.

Many efforts have been devoted to incorporate functionality within either the polymer or the surfactant building blocks, which can then be utilized or expressed in the final self-assembled material.[12–14] To date, almost all discoveries regarding polyelectrolyte–surfactant complexes involve organic polyelectrolytes,[15,16] with the exception of a number of studies by Thünemann *et al.* on Si-containing polymer–amphiphile systems.[4,17] Studies of metallopolymer–amphiphile systems, where metal centers introduce additional functionality,[18] are virtually unexplored.[19] In this work we have used well-studied polyferrocenylsilane (PFS) polyelectrolytes as one of the starting tectons for achieving this goal. These metallopolymers possess a variety of interesting properties making them very useful candidates for numerous applications. For example, PFS materials possess high refractive indices, etch resistance to plasmas, and function as precursors to ceramics with magnetic and

[a]*School of Chemistry, University of Bristol, Bristol, BS8 1TS, UK. E-mail: ian.manners@bristol.ac.uk; Fax: +44 (0)117 929 0509; charl.faul@bristol.ac.uk; Fax: +44 (0)117 925 1295; Tel: +44 (0)117 925 1295*
[b]*Nara National College of Technology, 22 Yatacho, Yamato-Koriyama, Nara, 639-1080, Japan*
[c]*Department of Applied Physics, Aalto University School of Science and Technology, P.O.Box 15100, FI-00076 Aalto, Finland*

catalytic properties.[20–23] Furthermore, a key attribute of PFS that would be of exceptional interest for materials prepared by ISA is its redox behaviour,[20,24] which involves the ability to reversibly switch between the Fe(II) and Fe(III) states. PFS polyelectrolytes were first reported around 2000, and have been widely exploited over the past decade owing to their excellent solubility in water and their redox properties.[25–28] For example, Vancso and Möhwald *et al.* have employed the layer-by-layer approach using PFS polyelectrolytes to form porous microcapsules with control of the capsule permeability by a redox-stimulus.[29] In addition, a similar approach has been used to create redox-tunable defects in photonic crystals.[30]

In this study, redox-active ISA materials were prepared from the complexation of three cationic PFS polyelectrolytes **qP1–qP3** with two different surfactants; bis-2-ethylhexyl sulfosuccinate (**AOT**) and an azobenzene surfactant (**azoB$_{12}$**) (see Chart 1). The interaction between cationic PFS polyelectrolytes and anionic surfactants was interrogated by FTIR spectroscopy and the materials were further characterized using small- and wide-angle X-ray scattering (SAXS, WAXS), transmission electron microscopy (TEM), thermogravimetric analysis (TGA), differential scanning calorimetry (DSC), polarized optical microscopy (POM), UV-vis spectrometry, and cyclic voltammetry (CV). The study focussed on the effects of changes in the structure of both the PFS polyelectrolyte and the surfactants on the mesomorphic phases formed. A key aim was to prepare mesostructures exhibiting redox switching behaviour. During the course of our work Ren, Tong and co-workers reported independent studies of polyelectrolyte-surfactant complexes formed by an alternative cationic PFS polyelectrolyte with a series of dendritic anionic surfactants.[19] Comparisons of their results with those from our study will also be provided.

2. Experimental

2.1 Materials and samples

Solvents were dried according to standard methods. Organosilanes were distilled prior to use. Ferrocene was used in a ground form generated from pellets received from Octel Germany. Tetramethylethylenediamine was distilled from CaH_2 and n-butyllithium was used as received from Aldrich. Hexanes and diethyl ether were purified using Anhydrous Engineering double alumina and alumina/copper catalyst drying columns. Methanol, used for quenching of the living polymer chains, was deoxygenated by nitrogen bubbling, and then degassed. Tetrahydrofuran was distilled from Na/benzophenone under reduced pressure prior to each experiment.

2.2 Synthesis of the PFS polyelectrolytes and surfactants

Three different PFS polyelectrolytes **qP1**, **qP2** and **qP3** (see Chart 1) were synthesized (in accordance to previous published methods[28,31]) in order to investigate the effect of the position and distance of the cationic charge (with respect to the polymer backbone) on the overall complexation with anionic surfactants. Each polyelectrolyte was synthesized with pendant cationic charged groups at different positions after quaternization. Due to the close proximity of the $-NMe_2$ group to the iron centre in the *ortho*-substituted monomer (which polymerizes to yield **P1**), the only viable polymerization method to prepare high molecular weight PFS polymer **P1** was thermal ring-opening polymerization (ROP). Therefore, this route resulted in polymer **P1** with very high molecular weight and a broad polydispersity, due to the lack of control this ROP method exhibits. Fortunately, the location of the $-NMe_2$ groups within the monomer precursors

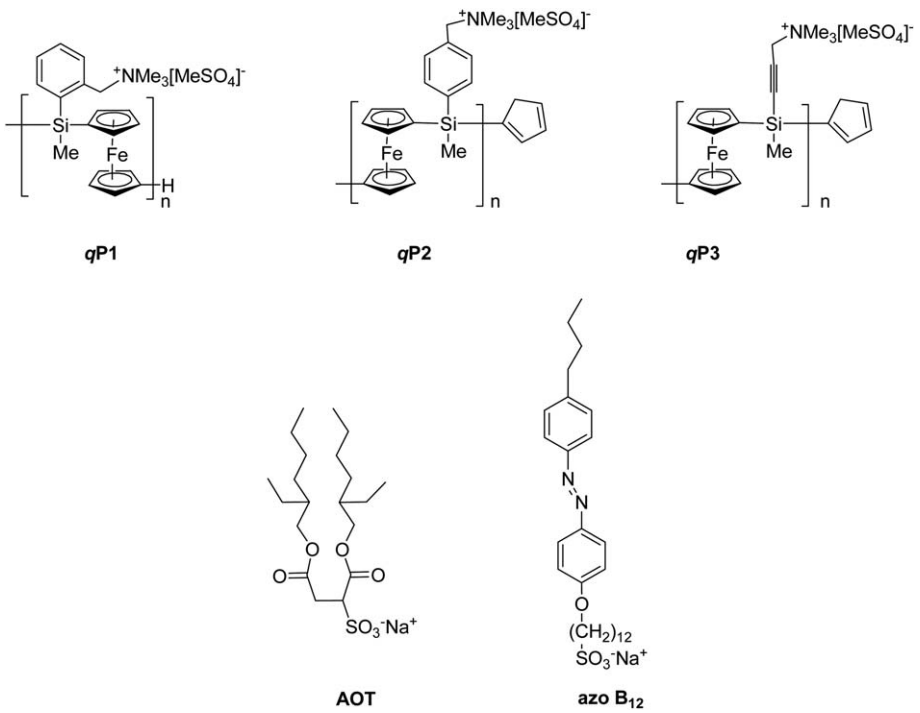

Chart 1 Structures of the polyelectrolytes **qP1–qP3** and the anionic surfactants; **AOT** and **azoB$_{12}$**.

for both **P2** and **P3** were further away from the iron centre, which enabled the use of the "living" photolytic ROP technique, resulting in polymers with controlled molecular weights and narrow polydispersities. Table 1 presents the characterization data of the polyelectrolytes used in this study. The number average molecular weight (M_n) of the PFS homopolymers (prior to quaternization) was determined using conventional GPC analysis (relative to polystyrene standards) using THF with additional Bu_4NBr as the eluent. **AOT** was purchased from Sigma-Aldrich and **azo B12** was synthesized using literature procedures.[32,33] All other chemicals were purchased from Sigma-Aldrich unless otherwise specified.

2.3 Complexation of cationic polyferrocenylsilane (PFS) polyelectrolytes and surfactants

Both the polyelectrolyte and the surfactant were dissolved separately in deionized water (1 wt %, 70 °C) respectively, to yield two 1% (by weight) solutions. After complete dissolution, the surfactant solution was added slowly, dropwise to the polyelectrolyte solution. The amount of surfactant added to the polyelectrolyte solution was strictly at a 1 : 1 charge stoichiometry, based on the expectation that the surfactant would selectively interact with quaternized amino-functionalized PFS through ionic interactions. The mixture was allowed to stir overnight, ensuring that there was a minimum amount of solvent loss by evaporation. All of the self-assembled cationic PFS polyelectrolyte–anionic surfactant materials were then collected by precipitation. The complete complexation between the PFS polyelectrolytes and anionic surfactants in these materials was visually observed by the change in colour of the corresponding solution from yellow to transparent. The formation of precipitates in deionized water (due to charge neutralization between the oppositely charged tectons) and resulting clear supernatant indicated successful complexation. The charge neutralized complexes were then washed several times with hot deionized water (to remove any $NaMeSO_4$ salts and unreacted surfactant) and dried under vacuum (40 °C, 1×10^{-2} mmHg) for 30 min. These materials were then readily soluble in common organic solvents such as chloroform, THF and toluene. Complexation was further monitored using FTIR, which revealed a characteristic change in the vibrational frequency of the sulfonate group within the surfactant from 1050, 1175 and 1220 cm^{-1} (**AOT**) to 1041, 1188 and 1219 cm^{-1} (complex). Furthermore, the vibration at 1058 cm^{-1}, which corresponds to $MeSO_4^-$, disappeared after complexation. Elemental analysis showed a lower than expected value for carbon as a result of the ceramic formation of the PFS at high temperatures. For X-ray diffraction studies and TEM analysis, all the complexes were first dissolved in chloroform (a good solvent), which was then slowly evaporated overnight. These bulk films were then further solvent annealed in saturated chloroform atmosphere and then thermally annealed under vacuum (150 °C, 4 d), to reach the thermodynamically most stable morphology. Thin films of the complexes (for POM investigations) were prepared by dropcasting solutions of each complex from chloroform (2 mg mL^{-1}) onto a glass cover slip. After solvent evaporation, the thin films were then thermally annealed on the heating stage (130 °C, 5 d) to obtain the most thermodynamically stable organizations for optical microscopy studies.

Table 1 Characterization data for the polyelectrolytes synthesized (values based on pre-quaternized polymers)

Polymer	M_n (g mol^{-1})	PDI[a]	DP_n[b]
qP1	~300,000	~3	833
qP2	35,000	1.09	97
qP3	30,000	1.04	97

[a] Polydispersity index (PDI), calculated using M_w/M_n. [b] Number average degree of polymerization (DP_n), calculated using M_n/M_o (where M_o is the molecular mass of a repeat unit of the polymer).

2.4 Equipment

All manipulations of air-sensitive materials were performed under nitrogen atmosphere either in MBraun glove box or by using standard Schlenk line techniques. ^1H and ^{13}C NMR spectra were recorded on Varian spectrometers (lambda 300 and ecp 400) and referenced to deuterated solvents. Conventional gel permeation chromatography using THF salt Bu_4NBr was used for the dimethylamino-based polymers and block copolymers by using a Waters Associates 2690 separation module equipped with a column heater, in-line degasser, a High Performance Liquid Chromatography (HPLC) pump, and an autosampler. Polystyrene standards purchased from Aldrich and Viscotek were used for calibration. Molecular weights were estimated relative to polystyrene standards. The photoirradiation experiments were carried out using pyrex-glass-filtered emission ($\lambda > 300$ nm) from a 125 W high pressure Hg arc lamp (Photochemical Reactors Ltd). Thermal Analysis including Differential Scanning Calorimetry (DSC) and thermogravimetric analysis (TGA) analyses were performed on the Q100 & Q500 from TA instruments at heating/cooling rates of 10 °C min^{-1}. The DSC was coupled to a refrigerated cooling system (RCS90). SAXS experiments were performed using a Rigaku SAXS instrument with an 18 kW rotating anode X-ray generator (MicroMax-002$^+$) equipped with a Cu tube operated at 45 kV and 0.88 mA. Wide-angle X-ray scattering (WAXS) was performed on a Bruker D8 powder diffractometer. The wavelength of the X-ray beam was 0.15418 nm. SAXS profiles were calibrated using silver behenate with the first-order scattering vector q being 1.076 nm^{-1} ($q = 4\pi\sin\theta/\lambda$, where λ is the wavelength and 2θ is the scattering angle). 1D WAXD profiles were calibrated using α-Al_2O_3 with known crystal diffraction at $2\theta = 28.47°$. The typical size of those PFS-surfactant complexes for the SAXS and WAXD measurements was $1.0 \times 1.0 \times 1.0$ mm^3. An exposure time of 60 min was required to obtain high-quality SAXS and WAXS diffraction profiles. Bulk samples for Transmission Electron Microscopy (TEM) analysis were microtomed at room temperature using a RMC MTXL ultramicrotome and a diamond knife. Copper grids from Agar Scientific (mesh 400) were coated with carbon film. TEM was performed on Jeol 1200EX TEM Mk2 which operates with a tungsten filament operated at 120 kV. It is fitted with a MegaViewII digital camera, using Soft Imaging Systems GmbH analySIS 3.0 image analysis software.

The one-dimensional (1D) correlation function ($\gamma(z)$) of lamellar PFS–surfactant complex in real space derived from the

Fourier transform of the one-dimensional SAXS profiles ($I(q)$ *versus* q) was introduced for precisely measuring the individual thickness of the PFS polymer layer, the surfactant layer, and the overall long period ($L = d_{PFS} + d_{surf}$). The one-dimensional correlation function is defined as

$$\gamma(z) = \frac{1}{\gamma(0)}\int_0^\infty I(q)q^2\cos(qz)dq \quad (1)$$

where z is the direction along which the electron density is measured and $\gamma(0)$ is just the scattering invariant:

$$\gamma(0) = \int_0^\infty I(q)q^2dq \quad (2)$$

Due to the finite q range of experimental SAXS data (q = 1.4–11 nm^{-1}), extrapolation of the 1D azimuthal scan SAXS data to both the low and high q regions were required for the integration of the intensity, I(q). Extrapolation to $q(0)$ was achieved by linear extrapolation, and extension of the intensity to large q values was accomplished by using the Porod-Ruland model.[34–37] The one-dimensional correlation function was measured after subtracting the background intensity arising from thermal density fluctuations from the overall intensity. The position of the first maximum determined the long period value (L), and the intersection of the baseline with the straight line extended from the self-correlation triangle was measured as the thinner layer thickness, or the PFS polymer layer thickness.

Photomicrographs of the four PFS polyelectrolyte–surfactant complexes were taken using an Olympus B50 polarized optical microscope (POM) fitted with a 5 mega pixel digital camera. Temperature-dependent measurements the PFS polyelectrolyte–surfactant complexes were performed using a Linkam TP92 Heater with THMS 600 heating stage at heating/cooling the sample at a rate of 10 °C/min. Electrochemical studies were carried out using an EG&G model 273A potentiostat linked to a computer using EG&G Model 270 Research Electrochemistry software in conjunction with a three-electrode cell. The working electrode was a platinum disc (1.6 mm diameter) and the auxiliary electrode a platinum wire. The reference was an aqueous saturated calomel electrode separated from the test solution by a fine porosity frit and an agar bridge saturated with KCl. Solutions of the polyelectrolyte–surfactant complexes were 2.0×10^{-3} M and NBu_4PF_6 (0.1 M) as the supporting electrolyte, the solvent used was degassed acetonitrile:methylene chloride (1 : 1). UV-vis profiles were obtained on a Lambda 35 spectrometer employing standard quartz cells (1 cm) from 200 to 800 nm at a scan rate of 2 nm s^{-1}.

3. Results and discussion

3.1 Formation of mesomorphic phases *via* ionic self-assembly

3.1.1 Influence of the polyelectrolyte charge location. In this section, the effects of changing the position of the cationic $-[NMe_3]^+$ group on the resulting mesomorphic phases were systematically investigated. Fig. 1a shows the POM micrograph of the complex formed between the **AOT** surfactant and the polyelectrolyte **qP1** (referred to as **qP1-AOT**). This result showed that birefringent materials were produced, indicating the presence of ordered mesomorphic structures, despite the high M_w (see Experimental section) and location of the *ortho*-charge position within the polyelectrolyte **qP1**, where its close proximity to the polymer backbone was likely to hinder the ability of the surfactant to efficiently bind electrostatically to the cationic side-arm of **qP1**, POM studies showed the formation of mesostructured materials. The mesomorphic nature was further confirmed by 1D SAXS profile (Fig. 1b) showing the scattering peak at the range of q = 2.5–3.5 nm^{-1} indicative of low-ordered nanostructured material.

We then investigated the effect of changing the position of the cationic ammonium group on the ability to form ISA complexes. Fig. 2a and 2b display the POM micrographs of the **qP2-AOT** complex. As expected, complexation of **qP2** with **AOT** resulted in materials that exhibited birefringent textures under crossed polarizers at room temperature, indicating the formation of mesostructured materials. The **qP2-AOT** complex reached an isotropic state after heating to 80 °C (note: the formed textures remained very small even after prolonged thermal annealing, which made identification of the phase from the textures difficult). A noticeable change in texture (under crossed polarizers) was detected when the temperature reached 80 °C, indicative of an anisotropic to isotropic phase transition. At this temperature, most of the liquid crystal-like mesophase melted and resulted in the formation of an isotropic phase (Fig. 2b). The phase behaviour of the material was further confirmed using DSC as shown in Fig. 2c. The thermogram showed a broad endotherm at 70 °C, which was assigned to the anisotropic to isotropic phase transition region. The corresponding enthalpy of the phase transition $\Delta H^{qP2\text{-}AOT}$ = 29.67 J g^{-1}, and falls within the range found for smectic-isotropic phase changes in supramolecular systems.[38] The thermal stability of the complex **qP2-AOT** was determined using TGA, which revealed a degradation temperature of 180 °C.

To gain further insight into the structural organization within these nanostructured materials, 1D WAXS and SAXS measurements were performed. WAXS profiles for **qP1-AOT** and **qP2-AOT** (Fig. 3a) showed a broad amorphous halo around $2\theta = 18°$ (d = 0.49 nm) and 19° (d = 0.47 nm) respectively, which is characteristic of a liquid-like arrangement of the surfactant alkyl tails.[39] The organization in the microphase-separated domains present within the **qP2-AOT** complex was further probed by 1D SAXS. Fig. 3b shows the 1D SAXS profile of **qP2-AOT** at room temperature. Analogous to the SAXS result for **qP1-AOT**, the **qP2-AOT** material exhibited only one scattering peak (q = 2.95 nm^{-1}, d = 2.13 nm) and other corresponding higher ordered scattering peaks were not observed. Similar results were also reported for organic poly(styrenesulfonate)–surfactant complexes,[2,40] whereby the presence of higher order scattering peaks (indicative of a lamellar structure) were missing. In our case, the absence of higher ordered peaks suggest that the PFS–surfactant complexes do not form long-range ordered structures (as also evidenced by the absence of large domains from PLM investigations). The low chain mobility in the PFS chain due to the existence of rigid, bulky metal-containing ferrocene groups might cause the formation of small domains of lamellar mesomorphic structures.[41] As no sharp diffraction peaks were observed in the wide-angle region, it was concluded that the alkyl tails in the surfactant layer are liquid like, *i.e.*, they do not crystallize in these materials. To gain further insight on the

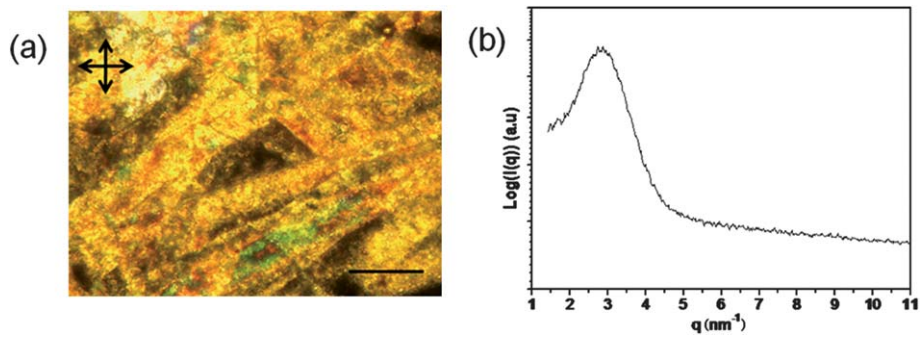

Fig. 1 (a) Polarized optical micrograph of the **qP1-AOT** complex at $T = 25$ °C (scale bar = 0.1 mm), (b) the corresponding 1D SAXS profile at room temperature.

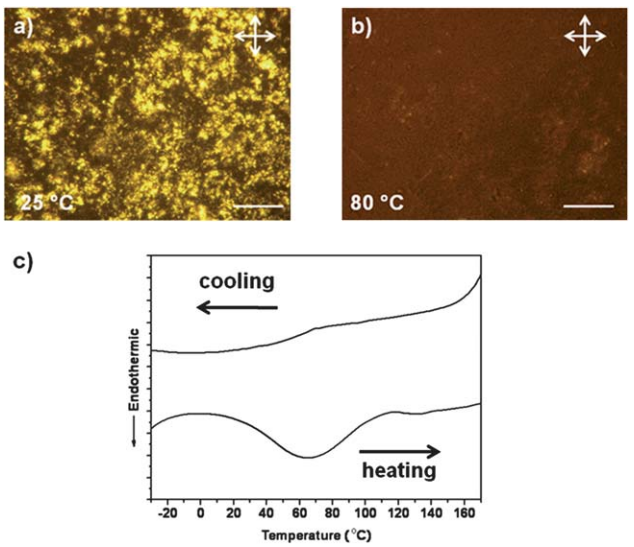

Fig. 2 (a) POM micrographs of the **qP2-AOT** complex at $T = 25$ °C, (b) $T = 80$ °C (scale bar = 0.1 mm). (c) DSC thermogram of the complex (heating rate: 10 °C min^{-1}).

mesophase morphology, transmission electron microscopy (TEM) was performed. Ultrathin sections were prepared by room-temperature microtoming of samples mounted on an epoxy resin using cyanoacrylate glue. The bright-field TEM image of the unstained **qP2-AOT** complex is shown in Fig. 2c and depicts a lamellar morphology with average periodicities of 2–3 nm, which corresponds to the values obtained from SAXS studies. The high electron density of the Fe-containing PFAMS block provides sufficient contrast for TEM imaging without staining and we assign the dark domains to be PFS and the lighter to be the **AOT** layer. The SAXS profile therefore provides, in conjunction with our TEM investigations, evidence for the formation of a low-ordered lamellar morphology.

To further confirm the respective thicknesses of the PFS and surfactant layers as well as the degree of order within the two complexes, one-dimensional correlation functions ($\gamma(z)$) were generated by performing a Fourier transform of the 1D SAXS profiles. Fig. 3d shows the one-dimensional correlation function for both **qP1-AOT** and **qP2-AOT** calculated from data collected at 25 °C. The position of the first maximum represents the average thickness $d_{total} = 1.90$ nm for the **qP1-AOT** complex ($d_{total} = 1.98$ nm for the **qP2-AOT** complex; this d_{total} value, calculated from the SAXS scattering peak, was considered as the weight-average value).[34,42] The intersection of the baseline and straight line extended from the self-correlation triangle corresponds to the average thickness of the thinner layer. This value of 0.87 nm is considered as the thicknesses of the organometallic PFS layer (d_{PFS}) for **qP1-AOT**, with $d_{PFS} = 0.90$ nm for **qP2-AOT** (as the weight fraction of PFS blocks (w_{PFS}) is lower than 0.5 in the PFS–surfactant complexes). This result indicates that the thickness of the surfactant layer, d_{AOT}, is 1.03 nm for **qP1-AOT** ($d_{AOT} = 1.08$ nm for **qP2-AOT**). In comparison to the fully stretched length of one AOT molecule (1.20 nm), this would indicate a very high degree of interdigitation of the alkyl tails within the two ISA complexes. It is concluded that the thicknesses of both the PFS and surfactant layers are similar for both complexes. However, the 1D correlation function for **qP1-AOT** exhibited more rapid decay in the probing direction (z-direction) than that of the **qP2-AOT**, indicating the formation of a less ordered lamellar microstructure for **qP1-AOT**. For the **qP2-AOT** complex, the position of the *para* cationic $-[NMe_3]^+$ seems to facilitate the formation of a more ordered lamellar mesophase structure as a result of the ease of ionic bond formation between the cationic PFS polyelectrolyte and anionic surfactant.

It is mentioned that the calculation of $\gamma(z)$ is based on a lamellar two phase model, which assumes that sharp interfaces exist between the two sublayers in the complex.[43,44] The formation of such ordered lamellar morphologies with a considerable amount of alkyl tail interdigitation is illustrated in Scheme 1. Such structures are similar to those proposed for cationic PFS polyelectrolyte-dendritic surfactant complexes reported by Ren, Tong and co-workers.[19] In their case, the structure was observed to become more ordered with an increase in the generation number of the dendritic surfactant. Nevertheless, in contrast to the observation of multiphase behaviour, including glassy, crystalline and liquid-crystalline states in the PFS polyelectrolyte-dendritic surfactant complexes,[19] a crystalline phase does not exist in these **PFS-AOT** complexes. It is speculated that both the low chain mobility due to the existence of rigid, bulky ferrocene groups in the PFS chain and asymmetric flexible alkyl tails associated with the existence of branched ethyl groups within the **AOT** surfactant significantly inhibit efficient packing, thereby preventing the formation of crystalline phases.

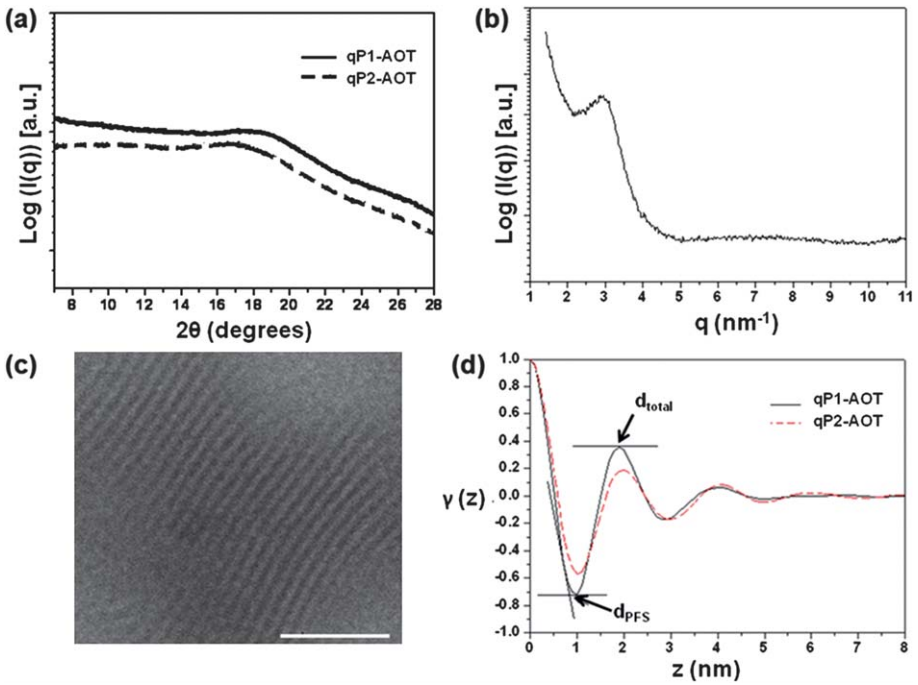

Fig. 3 (a) 1D WAXS diffractogram of the **qP1-AOT** and **qP2-AOT** complexes, (b) 1D SAXS pattern of **qP2-AOT** exhibiting ordered mesostructure and (c) TEM micrograph of **qP2-AOT** (scale bar 20 nm). (d) One-dimensional correlation functions of the **qP1-AOT** and **qP2-AOT** complex. All diffraction profiles were collected at room temperature.

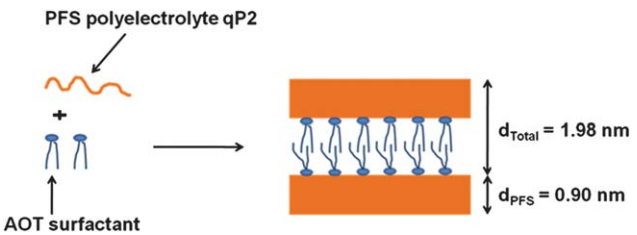

Scheme 1 Formation of ordered mesophases from **qP2-AOT** complex.

3.1.2 The influence of the surfactant structure. Next, we probed the role of changes within the surfactant's molecular architecture on the resulting mesomorphic state. Two different surfactants (**AOT** and **azoB$_{12}$**) were chosen to form the complexes with the **qP3** PFS polyelectrolyte. The azobenzene-based surfactant was utilized to investigate the effect of a long spacer group on the liquid-crystalline behaviour of the ISA complex. Moreover, the use of a light-sensitive tecton would allow potential structural changes within the material as a result of the photoisomerization mechanism within the azobenzene. Fig. 4 shows the POM micrographs and the corresponding DSC thermograms of the **qP3-AOT** and **qP3-azoB$_{12}$** complexes. POM investigations of the **qP3-AOT** complex showed birefringent textures at both room temperature and 70 °C (Fig. 4a, 4b), indicating the presence of anisotropic materials. Although the DSC thermogram showed a broad endotherm peak at $T = 56$ °C (Fig. 4e) ($\Delta H^{qP3\text{-}AOT} = 20.95$ J g^{-1}),[38] no distinct change in texture was observed from POM investigations, indicating this liquid-crystalline state was thermally stable and maintained over a wide temperature range.

POM micrographs for **qP3-azoB$_{12}$** also showed highly birefringent textures at room temperature, as shown in Fig. 4c. Upon heating, this ISA complex underwent a phase transition between 144–148 °C yielding a phase that exhibited a lower degree of birefringence (Fig. 4d). This phase transition was also observed in the DSC thermogram (Fig. 4f) as an endothermic transition at 148 °C ($\Delta H^{qP3\text{-}azoB}{}_{12} = 11.41$ J g^{-1}). Both temperature-dependent POM and DSC studies suggested that both **qP3-AOT** and **qP3-azoB$_{12}$** complexes exhibit thermotropic liquid-crystalline behaviour, which was further verified by X-ray diffraction studies.

Structural characterization and conformational ordering of the alkyl tails were investigated using X-ray diffraction studies at room temperature. Analogous to **qP2-AOT**, **qP3-AOT** showed an amorphous halo in the wide-angle region (Fig. 5a). This broad reflection at $2\theta = 18°$, with a calculated spacing of 0.49 nm, corresponds to the lateral packing of the alkyl chains, indicative of close (but not crystalline) packing of the alkyl tails upon complexation. WAXS studies of **qP3-azoB$_{12}$** (Fig. 5a) confirmed the presence of alkyl tail interactions as seen from the broad features in the range $2\theta = 17.7°$–$22°$. Furthermore, evidence for π–π interactions from the azobenzene moiety was observed at $2\theta = 25°$ corresponding to a typical stacking distance of 0.36 nm. Note that the diffraction profile of the blank **azo-B$_{12}$** surfactant showed a number of diffraction peaks, indicative of highly crystalline material.

SAXS studies of both the **qP3-AOT** and **qP3-azoB$_{12}$** complexes (Fig. 5b) exhibited similar scattering patterns as found for **qP1-AOT** and **qP2-AOT**. Once again, only one scattering peak was observed and other corresponding higher ordered scattering peaks were absent. Using similar arguments as above,

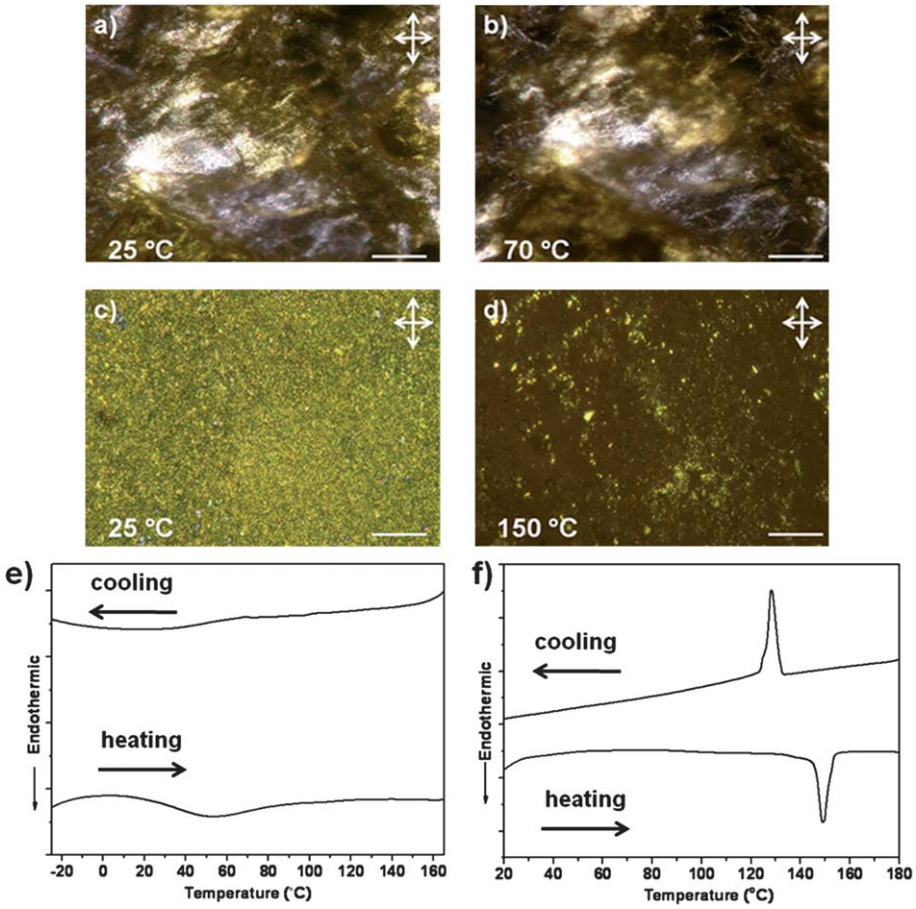

Fig. 4 (a) POM micrographs of the **qP3-AOT** complex at $T = 25$ °C, (b) $T = 70$ °C, (c) POM micrographs of the **qP3-azoB$_{12}$** complex at $T = 25$ °C, (d) $T = 150$ °C (scale bar = 0.1 mm) and (e) DSC thermogram of ISA complex **qP3-AOT** and f) **qP3-azoB$_{12}$** (heating rate: 10 °C min^{-1}).

we expect these two complexes to form weakly organized lamellar phases. The average d-spacing for both **qP3-AOT** and **qP3-azoB$_{12}$** were 2.1 nm and 2.0 nm respectively (Fig. 5b). The SAXS data for **qP3-azoB$_{12}$** indicated the high level of surfactant tail interdigitation present within the complex. Furthermore, in order to facilitate a d-spacing of 2 nm, a high degree of tilt of the **azoB$_{12}$** alkyl chains (within the lamellar layer) must occur (see Fig. 5f for a schematic representation). TEM analysis of both complexes provided additional evidence of the lamellar mesophase formation, as seen in Fig. 5c–d. The average d-spacings observed from TEM analysis corresponded to the values obtained from SAXS studies. Detailed structural information and the degree of order for these ISA complexes could be extracted from the one dimensional correlation function shown in Fig. 5e. It showed a total d-spacing (d_{total}) of 2.0 nm and $d_{PFS} = 0.97$ nm for the **qP3-azoB$_{12}$** complex and $d_{total} = 1.94$ nm and $d_{PFS} = 0.89$ nm for the **qP3-AOT** complex. Furthermore, the 1D correlation function of the **qP3-AOT** complex exhibited more rapid decay in the probing direction (z-direction) than that of the **qP3-azoB$_{12}$** complex, indicating the formation of a more ordered lamellar microstructure in the **qP3-azoB$_{12}$** complex. The rigid azobenzene group and the possibilities for π–π interactions seem to facilitate the formation of a more ordered lamellar mesophase structure than found for the **qP3-AOT** complex. These structural features however did not lead to the formation of overall highly ordered structures.

The UV-vis spectrum (Fig. 6) of the **qP3-azoB$_{12}$** complex (THF, 1×10^{-6} M) showed an absorbance maximum at 354 nm, characteristic of the azobenzene moiety. The very small bathochromic shift of 9 nm in the UV-vis spectrum of the complex with respect to the absorbance maximum of the pure azobenzene tecton (345 nm, THF 1×10^{-6} M), suggests only a small change in the way the chromophores interact. The shoulder at 440 nm was attributed to the PFS and was similar to the Laporte forbidden *d-d* transitions seen for ferrocene.[45]

The characterization data for both **qP3-AOT** and **qP3-azoB$_{12}$** indicated the presence of liquid-crystalline PFS-based materials with ordered mesostructures. Furthermore, from X-ray studies, the surfactants' molecular architecture did not influence the d-spacing of the overall lamellar mesomorphic nanostructure. In addition, the **qP3-azoB$_{12}$** complex contains a photoisomerisable side group, which can potentially be utilized for the formation of photoresponsive ISA materials.[46,47]

3.1.3 Redox chemistry of the ISA complexes qP1-AOT, qP2-AOT and qP3-AOT. Cyclic voltammetry (CV) was performed to investigate the redox behaviour of these PFS-containing complexes in solution (10 mg mL^{-1}). Fig. 7 shows the

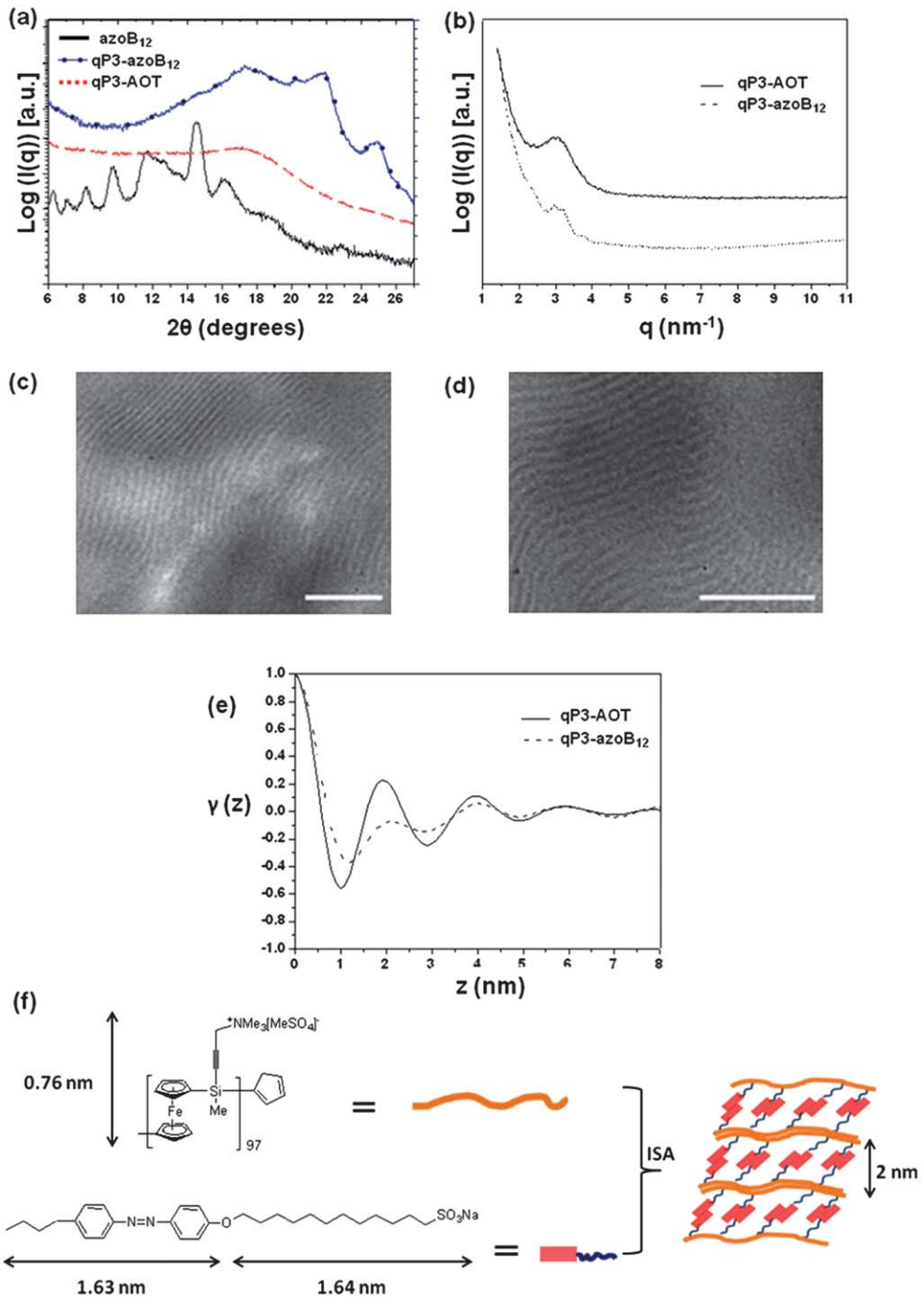

Fig. 5 (a) 1D WAXS diffractogram of **qP3-AOT** and **qP3-azoB$_{12}$** and **azoB$_{12}$**, (b) 1d SAXS diffractograms of **qP3-AOT** and **qP3-azoB$_{12}$**, (c) TEM micrograph of **qP3-AOT** and (d) TEM micrograph of **qP3-azoB$_{12}$** (scale bar: 20 nm), (e) one-dimensional correlation functions of **qP3-AOT** and **qP3-azoB$_{12}$** complexes. All diffraction profiles were collected at room temperature, (f) schematic illustration for the formation of a lamellar organization by the **qP3-azoB$_{12}$** complex.

solution-based cyclic voltammograms of **qP1-AOT**, **qP2-AOT** and **qP3-AOT**. All 3 complexes exhibited two peaks during the oxidation/reduction sweeps. This is a characteristic trait of PFS polymers,[24] which is a consequence of the presence of iron-iron interactions along the polymer backbone. Thus, oxidation of an iron centre leads to an increase in the oxidation potential of the next nearest neighbours, which therefore oxidize at a higher redox potential. A mixed solvent system consisting of CH_3CN/CH_2Cl_2 (50 : 50) was necessary to facilitate the solubilization of both the oxidized and non-oxidized species.[48]

Further investigations were undertaken using **qP3-AOT** to observe how these complexed ISA materials behaved under the influence of oxidants and reductants. We conducted initial solution studies of **qP3-AOT** (2 mg mL^{-1}, THF) with controlled

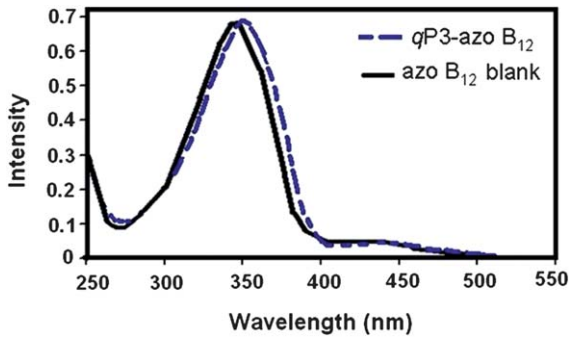

Fig. 6 UV-Vis spectra of the **qP3-azoB$_{12}$** complex and **azoB$_{12}$** blank (THF, 1×10^{-6} M).

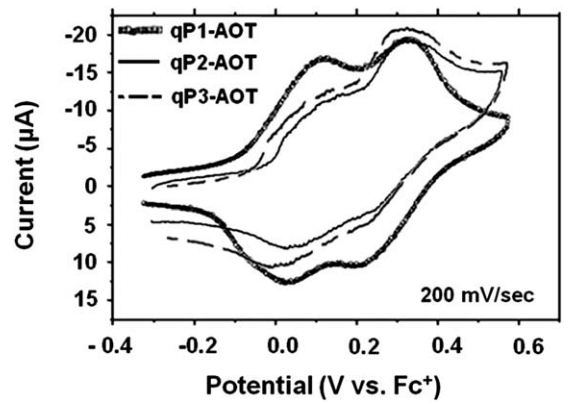

Fig. 7 Cyclic voltammograms of **qP1-AOT**, **qP2-AOT** and **qP3-AOT**, electrolyte used: NBu_4PF_6, solvent used: (50 : 50 CH_3CN:CH_2Cl_2).

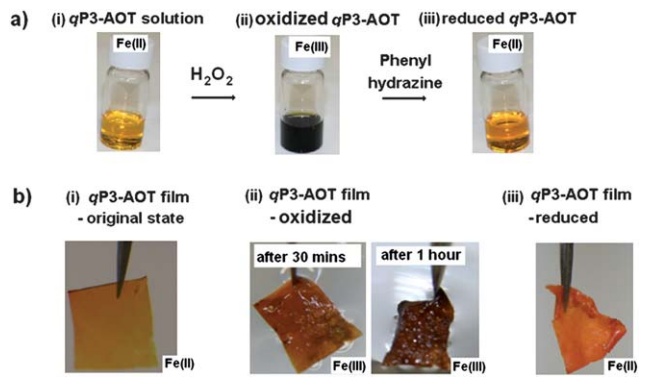

Fig. 8 Redox studies of **qP3-AOT**: both (a) solution studies and (b) film studies.

amounts of oxidants and reductants (50 μL of 10 wt % $FeCl_3$ solutions and 50 μL of 10 wt % phenylhydrazine solution in THF). Fig. 8a depicts the colour change (from amber to dark green) of the solution upon treatment with $FeCl_3$, in which an obvious oxidation of the Fe centres in the PFS backbone takes place resulting in oxidized Fe(III) centres. This state can readily be reduced using, for example, phenylhydrazine, which reduces the Fe(III) state back to the Fe(II) state. Once again, this change can be visualized by a colour change of the solution from dark green back to amber.

Redox chemistry studies of the **qP3-AOT** film, as shown in Fig. 8b, indicated that the material exhibited similar redox behaviour to that in the solution state (Fig. 8a). However, in this particular case, immersing the hydrophobic films in aqueous hydrogen peroxide solution (10 wt % solution, 1 h) led to oxidation and induced a change in both shape and colour (from amber to brown). This was presumably a result from stresses caused by the resulting oxidation process and counteranion incorporation and also swelling arising from the increase in hydrophilicity. Reduction in the presence of ascorbic acid solution (1 M, 1 h) changed the colour of the film back to amber, indicative of the Fe(II) state.

4. Summary

New redox-active mesostructures were prepared by ionic self-assembly of PFS polyelectrolytes and anionic surfactants. These complexes exhibited ordered mesomorphic, but non-crystalline structures and showed thermotropic liquid-crystalline characteristics. It was shown that the accessibility of charge, and thus the design of polyelectrolyte architecture, played an important role in the degree of ordering within the resulting mesomorphic complexes. The choice of surfactant (both in terms of architecture and function) contributed to the ability to design complexes with liquid-crystalline properties and results showed that the surfactant's molecular architecture did not govern the d-spacing of the overall mesomorphic state. Additional functionality, such as photo-addressability, was easily introduced and the resulting photoactive materials have potential as stimuli-responsive systems. Finally, the inclusion of redox-active PFS materials into ISA complexes was shown to provide a facile route to the formation of materials which exhibit redox reversibility, an attribute that may be useful in future applications.

Acknowledgements

M.-S. H thanks the European Union for a Marie Curie Fellowship. I. M. thanks EPSRC and the EU for financial support. C. F. J. Faul thanks the University of Bristol for financial support.

References

1 S. Q. Zhou and B. Chu, *Adv. Mater.*, 2000, **12**, 545.
2 M. Antonietti, J. Conrad and A. Thünemann, *Macromolecules*, 1994, **27**, 6007.
3 A. F. Thünemann, D. Ruppelt, H. Schnablegger and J. Blaul, *Macromolecules*, 2000, **33**, 2124.
4 A. F. Thünemann, *Prog. Polym. Sci.*, 2002, **27**, 1473.
5 M. Antonietti and J. Conrad, *Angew. Chem., Int. Ed. Engl.*, 1994, **33**, 1869.
6 C. K. Ober and G. Wegner, *Adv. Mater.*, 1997, **9**, 17.
7 N. Canilho, E. Kasemi, A. D. Schlüter, J. Ruokolainen and R. Mezzenga, *Macromol. Symp.*, 2008, **270**, 58.
8 A. Tiitu, J. Laine, R. Serimaa and O. Ikkala, *J. Colloid Interface Sci.*, 2006, **301**, 92.
9 C. F. J. Faul and M. Antonietti, *Adv. Mater.*, 2003, **15**, 673.
10 K. Thalberg and B. Lindman, in *Surfactants in Solution*, ed., K. L. Mittal and D. O. Shah, Springer, 1991, **vol. 11**, p.243.
11 G. H. Fredrickson, *Macromolecules*, 1993, **26**, 2825.
12 B. Y. Ren, Z. Tong, X. X. Liu, C. Y. Wang and F. Zeng, *Langmuir*, 2004, **20**, 10737.
13 Z. Y. Cheng, B. Y. Ren, M. Gao, X. X. Liu and Z. Tong, *Macromolecules*, 2007, **40**, 7638.

14 A. F. Thünemann and D. Ruppelt, *Langmuir*, 2000, **16**, 3221.
15 H. L. Chen and M. S. Hsiao, *Macromolecules*, 1999, **32**, 2967.
16 O. Ikkala and G. ten Brinke, *Science*, 2002, **295**, 2407.
17 A. F. Thünemann and K. H. Lochhaas, *Langmuir*, 1998, **14**, 6220.
18 G. R. Whittell and I. Manners, *Adv. Mater.*, 2007, **19**, 3439.
19 Z. Y. Cheng, B. Y. Ren, D. L. Zhao, X. X. Liu and Z. Tong, *Macromolecules*, 2009, **42**, 2762.
20 K. Kulbaba and I. Manners, *Macromol. Rapid Commun.*, 2001, **22**, 711.
21 J. C. Eloi, L. Chabanne, G. R. Whittell and I. Manners, *Mater. Today*, 2008, **11**, 28.
22 V. Bellas and M. Rehahn, *Angew. Chem., Int. Ed.*, 2007, **46**, 5082.
23 I. Korczagin, R. G. H. Lammertink, M. A. Hempenius, S. Golze and G. J. Vancso, *Adv. Polym. Sci.*, 2006, **200**, 91.
24 R. Rulkens, A. J. Lough, I. Manners, S. R. Lovelace, C. Grant and W. E. Geiger, *J. Am. Chem. Soc.*, 1996, **118**, 12683.
25 M. A. Hempenius, N. S. Robins, R. G. H. Lammertink and G. J. Vancso, *Macromol. Rapid Commun.*, 2001, **22**, 30.
26 K. N. Power-Billard and I. Manners, *Macromolecules*, 2000, **33**, 26.
27 Z. Wang, A. Lough and I. Manners, *Macromolecules*, 2002, **35**, 7669.
28 F. Jakle, Z. Wang and I. Manners, *Macromol. Rapid Commun.*, 2000, **21**, 1291.
29 Y. J. Ma, W. F. Dong, E. S. Kooij, M. A. Hempenius, H. Möhwald and G. J. Vancso, *Soft Matter*, 2007, **3**, 889.
30 F. Fleischhaker, A. C. Arsenault, Z. Wang, V. Kitaev, F. C. Peiris, G. V. Freymann, I. Manners, R. Zentel and G. A. Ozin, *Adv. Mater.*, 2005, **17**, 2455.
31 Z. Wang, G. Masson, F. C. Peiris, G. A. Ozin and I. Manners, *Chem.–Eur. J.*, 2007, **13**, 9372.
32 P. M. K. Hunger, W. Rieper, R. Rau, K. Kunde and A. Engel, *Ullmann's Encycl. Ind. Chem*, 1985.
33 R. M. Christie, *Colour Chemistry*, 2001.
34 C. G. Vonk, *J. Appl. Crystallogr.*, 1978, **11**, 541.
35 G. Porod, *Kolloid-Z.*, 1951, **124**, 83.
36 G. Porod, *Kolloid-Z.*, 1952, **125**, 51.
37 G. Porod, *Kolloid-Z.*, 1952, **125**, 108.
38 The enthalpy change for a smectic-isotropic liquid transition for polymer-based supramolecular systems has been reported at 20.2 J g^{-1}, thus providing further support for the proposed structural model. See T. Kato, H. Kihara, U. Kumar, T. Uryu and J. M. J. Frechet, *Angew. Chem., Int. Ed. Engl.*, 1994, **33**, 1644.
39 K. Okuyama, Y. Soboi, N. Iijima, K. Hirabayashi, T. Kunitake and T. Kajiyama, *Bull. Chem. Soc. Jpn.*, 1988, **61**, 1485.
40 K. Nakamura and K. Fukao, *Macromolecules*, 2011, **44**, 3053.
41 V. S. Papkov, M. V. Gerasimov, I. I. Dubovik, S. Sharma, V. V. Dementiev and K. H. Pannell, *Macromolecules*, 2000, **33**, 7107.
42 G. R. Strobl and M. Schneider, *J. Polym. Sci., Polym. Phys. Ed.*, 1980, **18**, 1343.
43 W. Ruland, *J. Appl. Crystallogr.*, 1971, **4**, 70.
44 W. Ruland and B. Smarsly, *J. Appl. Crystallogr.*, 2004, **37**, 575.
45 D. Foucher, R. Ziembinski, R. Petersen, J. Pudelski, M. Edwards, Y. Z. Ni, J. Massey, C. R. Jaeger, G. J. Vancso and I. Manners, *Macromolecules*, 1994, **27**, 3992.
46 Y. Zakrevskyy, J. Stumpe and C. F. J. Faul, *Adv. Mater.*, 2006, **18**, 2133.
47 O. Kulikovska, L. M. Goldenberg and J. Stumpe, *Chem. Mater.*, 2007, **19**, 3343.
48 It is worth noting that solid-state CV studies were performed. However, due to the low electron mobility and slow dynamics, the surfaces of the electrodes were partially coated with PFS residues, leading to distorted readings.